Enhanced Axon Outgrowth and Improved Long-Distance Axon Regeneration in Sprouty2 Deficient Mice

Letizia Marvaldi,[1] Sitthisak Thongrong,[1] Anna Kozłowska,[1]* Regina Irschick,[1] Christian O. Pritz,[2] Bastian Bäumer,[3] Giulia Ronchi,[4] Stefano Geuna,[4] Barbara Hausott,[1] Lars Klimaschewski[1]

[1] Division of Neuroanatomy, Department of Anatomy and Histology, Medical University Innsbruck, 6020 Innsbruck, Austria

[2] Department of Otolaryngology, Medical University Innsbruck, 6020 Innsbruck, Austria

[3] Division of Neurobiochemistry, Biocenter, Medical University Innsbruck, 6020 Innsbruck, Austria

[4] Neuroscience Institute of the Cavalieri Ottolenghi Foundation, University of Turin, TO 10043 Italy

Received 3 April 2014; revised 16 July 2014; accepted 6 August 2014

ABSTRACT: **Sprouty (Spry) proteins are negative feedback inhibitors of receptor tyrosine kinase signaling. Downregulation of Spry2 has been demonstrated to promote elongative axon growth of cultured peripheral and central neurons. Here, we analyzed Spry2 global knockout mice with respect to axon outgrowth *in vitro* and peripheral axon regeneration *in vivo*. Neurons dissociated from adult Spry2 deficient sensory ganglia revealed stronger extracellular signal-regulated kinase activation and enhanced axon outgrowth. Prominent axon elongation was observed in heterozygous Spry2$^{+/-}$ neuron cultures, whereas homozygous Spry2$^{-/-}$ neurons predominantly exhibited a branching phenotype. Following sciatic nerve crush, Spry2$^{+/-}$ mice recovered faster in motor but not sensory testing paradigms (Spry2$^{-/-}$ mice did not tolerate anesthesia required for nerve surgery). We attribute the improvement in the rotarod test to higher numbers of myelinated fibers in the regenerating sciatic nerve, higher densities of motor endplates in hind limb muscles and increased levels of GAP-43 mRNA, a downstream target of extracellular regulated kinase signaling. Conversely, homozygous Spry2$^{-/-}$ mice revealed enhanced mechanosensory function (von Frey's test) that was accompanied by an increased innervation of the epidermis, elevated numbers of nonmyelinated axons and more IB4-positive neurons in dorsal root ganglia. The present results corroborate the functional significance of receptor tyrosine kinase signaling inhibitors for axon outgrowth during development and nerve regeneration and propose Spry2 as a novel potential target for pharmacological inhibition to accelerate long-distance axon regeneration in injured peripheral nerves.** Develop Neurobiol 75: 217–231, 2015

Keywords: **innervation; sensory; motor; ganglion; axotomy; fibroblast growth factor; nerve growth factor**

INTRODUCTION

In contrast to the central nervous system, peripheral axons regenerate after injury mainly because of the more permissive environment. Yet, peripheral nerve

Additional Supporting Information may be found in the online version of this article.

**Present address:* Department of Human Physiology, Faculty of Medicine Sciences, University of Warmia and Mazury, Żołnierska 14C, Olsztyn, Poland.

Correspondence to: L. Klimaschewski, (lars.klimaschewski@i-med.ac.at)

Contract grant sponsor: Austrian Science Fund (to L.M.; FWF); contract grant number: W 1206-B18.

Contract grant sponsor: Med-El Innsbruck (to C.O.P.).

Published online 8 August 2014 in Wiley Online Library (wileyonlinelibrary.com).
DOI 10.1002/dneu.22224

lesions often cause persistent functional deficits that are at least partially due to extensive branching of regenerating axons at the lesion site (Gordon, 2009). Therefore, improvement of elongative axon growth is required for faster long-distance regeneration of axons to the skin and into target muscles, which atrophy in the absence of reinnervation.

Following injury to peripheral nerves approximately half of the affected neuron population sends out axons that enter glial guidance channels in response to secreted neurotrophins and other neuronal growth factors (Klimaschewski et al., 2013). These lesion-associated polypeptides create an environment that is highly supportive for axon regrowth and ensure that the majority of regenerating axons are directed toward the distal nerve stump. Unfortunately, however, most neurotrophic factors act as strong stimulators of axonal sprouting at the lesion site. Although some of the axon branches will withdraw at later stages, the sprouting effect contributes to the misdirection of reinnervation that results in lack of functional recovery observed in many patients with nerve injuries.

By activation of neuronal receptor tyrosine kinases, neurotrophic factors stimulate several signaling pathways that are involved in both, axon elongation and branching. However, the downstream molecular mechanisms affecting the axonal cytoskeleton are clearly different (Gallo, 2011). Sprouty (Spry) proteins belong to a group of negative feedback inhibitors of receptor tyrosine kinase signaling comprising four members (Mason et al., 2006). They are implicated in cellular proliferation and differentiation such as angiogenesis (Impagnatiello et al., 2001), branching morphogenesis (Tang et al., 2011) and brain development (Yu et al., 2011). Sprys function as growth factor antagonists, thereby fine-tuning receptor tyrosine kinase activities mainly by specific interference with processes upstream of extracellular signal-regulated kinase (ERK), although their precise biochemical mechanisms remain controversial (Mason, 2007).

In PC12 pheochromocytoma cells, overexpression of Spry1/2 blocks neurite outgrowth by nerve growth factor (NGF) or fibroblast growth factor (FGF-2; Gross et al., 2001). In contrast, nonphosphorylated dominant-negative Spry1/2 (Hanafusa et al., 2002) or Spry4 (Sasaki et al., 2001) potentiate FGF-2 induced neurite outgrowth. In the peripheral nervous system, downregulation of Spry2 induces axon outgrowth through enhanced Ras/Raf/ERK-signaling, whereas overexpression inhibits axon growth without affecting cell viability (Hausott et al., 2009).

The expression of Sprys is regulated by growth factors. In dorsal root ganglion (DRG) cultures, Spry1 is upregulated by FGF-2 and NGF, whereas Spry4 is induced by FGF-2 only (Hausott et al., 2009). In response to a peripheral nerve lesion, however, Spry mRNA levels do not change. Nevertheless, Spry2 is regulated post-transcriptionally, with Spry2 protein levels being reduced as a result of an induction of microRNA-21 (miR-21) following nerve injury *in vivo* (Strickland et al., 2011).

In this study, we set out to investigate axon outgrowth and nerve regeneration in Spry2 mutant mice as compared to wildtype (wt) mice *in vitro* and *in vivo*. The sciatic nerve, skin, and muscle innervation as well as functional recovery in response to nerve crush injury was assessed as an indicator for a possible inhibitory role of Spry2 during nerve development and peripheral nerve regeneration.

MATERIALS AND METHODS

Mutant Animals

Spry2-delta-ORF (*Spry2*$^{tm1.1Mrt}$/Mmnc) knockout mice were obtained from MMRRC (Mutant Mouse Regional Resource Centre, University of North Carolina at Chapel Hill) on a mixed genetic background. Backcrossing was performed on a 129 S1/SVImJ background until the tenth generation. By the time of weaning most Spry2$^{-/-}$ mice had died, and the remaining homozygous mice were smaller than normal as reported previously (Taketomi et al., 2005). As a result of their reduced weight, only few homozygous mice reached adult age, but they were not able to survive anesthesia required for nerve surgery. Therefore, lesion experiments were performed in Spry2$^{+/-}$ mice only.

Primary Neuron Cultures

Lumbar DRG were harvested from 8–10 weeks old mice as previously published (Andratsch et al., 2009). Following removal of connective tissue, ganglia were incubated in liberase blendzyme 1 (Roche, 9 mg/100 mL DMEM) for 60 min. After rinsing with phosphate-buffered saline (PBS), 1× trypsin-EDTA (Invitrogen) was added for 15 min, and DRG were washed with TNB 100TM medium (Biochrom) supplemented with L-glutamin (Invitrogen), penicillin G sodium, streptomycin-sulfate (Invitrogen), and protein-lipid-complexTM (Biochrom). Ganglia were dissociated with a fire-polished Pasteur pipette and centrifuged at low speed (10 min, 500 rpm) through a 3.5% bovine serum albumin (BSA) gradient (Sigma Aldrich) to minimize the number of non-neuronal cells. Neurons were resuspended, plated at a density of 50–80 per glass coverslip coated with poly-L-lysine/laminin (Sigma Aldrich) and cultivated in TNB medium at 37°C in 5% CO2 for 24 h in the presence of FGF-2 (Sigma) or mNGF 2.5S (Alomone Labs) if required. Superior cervical ganglion (SCG) neurons were obtained at postnatal day 5–7, dissociated, plated on a poly-L-ornithine/

laminin substrate and treated with 5 ng/mL NGF to maintain survival for 24 h as described before (Loy et al., 2011).

Immunocytochemistry and Histochemistry

After 24 h in culture, neurons were fixed with 4% paraformaldehyde (PFA) for 20 min, permeabilized with 0.01% Triton X-100 (Sigma Aldrich) in PBS for 5 min and blocked with blocking buffer (20% goat serum in PBS) for 30 min. Cells were incubated with primary antibodies against neuron-specific β-III Tubulin (TuJ1, R&D systems, 1:1000), pERK (Cell Signaling, 1:250), ERK (Cell Signaling, 1:250), Spry2 (Upstate, 1:200), CGRP (AbD SEROTEC, 1:200), S100 (Abcam, 1:200), GAP-43 (Millipore, 1:500), PGP 9.5 (gift from Anne Zurn, Lausanne, Switzerland, 1:2000), or with lectine IB4 (Invitrogen, 1:1000), all diluted in blocking buffer for 1 h at room temperature (RT), washed with PBS and incubated with secondary antibodies (Alexa-488 goat anti-rabbit, Alexa-594 chicken anti-mouse, Invitrogen, 1:1000) for 30 min at RT. Nuclei were stained with DAPI (1:1000 in PBS) and coverslips embedded in Moviol (Calbiochem).

For histology of sciatic nerves and sensory ganglia, tissues were fixed in 4% PFA overnight. Following three washes in PBS, specimens were incubated in 15% sucrose overnight, transferred to 100% OCT compound (TissueTek) and rapidly frozen in liquid nitrogen. For neuron counting, cryosections from the right lumbar DRG (L3–L5) and corresponding spinal cord segments of 8–10 weeks old mice were stained with cresyl violet. Nissl-positive neuronal profiles with nucleus were counted in every fifth section and numbers corrected according to Abercrombie's formula taking into account the section thickness and mean nuclear diameter (Abercrombie, 1943).

For immunolabeling, DRG and sciatic nerve cryosections (10 and 20 μm, respectively) were permeabilized with 0.3% Triton X-100 (Sigma Aldrich) and blocked with 5% BSA and 15% goat serum in PBS for 4 h at RT. Samples were then incubated with primary antibodies (same as above) overnight at 4°C followed by 1 h at RT, rinsed three times for 10 min in PBS and incubated with secondary antibodies (same as above) for 2 h at RT, rinsed and embedded with fluorescent mounting medium (Dako).

Following double-labeling immunofluorescence against GAP-43 and S100 on 20 μm cryosections of the sciatic nerve randomly chosen regions of interest (3570 μm^2) were measured and the mean intensity values determined after background subtraction. Confocal microscopy was performed with a Leica TCS SP5 microscope. Images were acquired with a 63× glycerol objective (N.A. 1.3) and imaging parameters for excitation and detection kept the same for all conditions (laser intensities: 405 diode - 15%, argon 488 - 12%, DPSS 561 - 10%).

For analysis of muscle innervation, the gastrocnemius muscle was dissected from perfusion fixed mice (4% PFA) at 7, 14, and 28 days after sciatic nerve crush, cryoprotected with 25% sucrose overnight, and frozen in OCT compound. Cryosections (50 μm) were stained with Alexa-Fluor-488-conjugated-α-bungarotoxin (Molecular Probes, 1:3000). Images were acquired with a 5× objective and the density of motor endplates determined (as number per area).

For analysis of epidermal sensory innervation, the glabrous hind paw skin was fixed for 1 h in 4% PFA, cryoprotected in 20% sucrose at 4°C for at least 24 h, embedded and frozen in optical cutting medium (OCT). Cryostat sections of 20 μm were processed for immunofluorescence as described above. Analysis of immunostaining was performed blinded to genotype. Images were processed using EMBL ImageJ (V1.45h, NIH) or Corel Photopaint X3 software. Quantification of epidermal sensory innervation density was performed as described before (Baumer et al., 2014). In brief, labeled nerve fibers in the epidermis of at least 10 randomly chosen confocal micrographs (20 μm stacks) of four animals per genotype were counted and the fiber density (# of fibers/1000 μm^2) was calculated. Epidermal thickness was determined in at least 10 randomly chosen confocal micrographs of four animals per genotype with the Leica Application Suite (LAS lite, version 2.6.0) and the fiber length was calculated by multiplying the epidermal thickness with the fiber density.

Fluorescently labeled cultured neurons and tissue sections were analyzed using confocal or conventional fluorescence microscopy (for pERK/ERK intensity measurements and axon morphometry). The longest vector from the center of the cell body to one of the growth cones (maximal distance), the number of all axonal branch points per neuron, and the total axonal length were determined for each neuron applying Metamorph (Visitron) and WIS-Neuromath software (Rishal et al., 2013). All morphologically intact neurons per dish with axons longer than two cell body diameters were analyzed (Klimaschewski et al., 2002). Evaluation of the average fluorescence intensity was performed after background subtraction (Bavassano et al., 2013) and images processed using Metamorph, Fiji bundle for ImageJ, and Adobe Illustrator CS5.

Quantitative RT-PCR

Under deep anesthesia, mice were sacrificed at days 1, 3, and 14 post injury and 7 mm of the sciatic nerve distal to the lesion were dissected. The corresponding portion of the right sciatic nerve served as internal control. For determination of Spry mRNAs in DRG naïve mice were used. All samples were immediately frozen in liquid nitrogen. The RNA was extracted using TRIzol reagent (Invitrogen) according to the manufacturer's instructions. Total RNA of 0.5 μg was subjected to a reverse transcriptase reaction in 25 μL reaction volume containing 1× buffer, 0.1 μg/μL BSA, 0.05% Triton X-100, 1 m*M* dNTPs, 7.5 μ*M* random hexanucleotide primers, 40 U RIBOlock, and 200 U RevertAid^{TM} M-MuLV reverse transcriptase (all by Fermentas). The reaction was performed for 10 min at 25°C, 90 min at 42°C, and 10 min at 90°C. Quantitative real-time PCR for GAP-43, β-actin, Sprouties, and the housekeeping gene TATA box binding protein (TBP) was performed using an ABI Prism 7300 (Applied Biosystems) detection system applying SYBR Green chemistry or fluorescent TaqMan

technology. cDNA was diluted 10 times before analysis and 5 μL were analyzed in a total volume of 20 μL. For each cDNA sample, three technical replicates were averaged. The reactions were carried out in 40 cycles (primer annealing temperature: 60°C). For β-actin and TBP, the reaction was performed in 1× PowerGREEN Master Mix (Applied Biosystems) and 300 n*M* forward and reverse primer. Dissociation curves were routinely performed to check for the presence of a single peak corresponding to the required amplicon. Normalized reporter fluorescence (Rn) for each cycle was obtained by normalizing SYBRGreen to the ROX signal. For GAP-43, the reaction was performed in 1× TaqMan® Universal PCR Master Mix and 1× TaqMan Gene Expression Assay (Applied Biosystem). The data from real-time PCR experiments were analyzed using the ΔΔCt method for relative quantification. Expression levels were normalized to the TBP. As calibrator the contralateral sciatic nerve was chosen. Primer sequences were: TBP forward 5′-GATCAAACCCAGAATTGTTCTCC-3′, TBP reverse 5′-GGGGTAGATGTTTTCAAATGCTTC-3′, β-actin forward 5′-CTTCTTTGCAGCTCCTTCGTTGCC-3′, β-actin reverse 5′GACGACCAGCGCAGCGATATC-3′, Spry1 forward 5′-CATGGCAGATTTCCGCTG-3′, Spry1 reverse 5′-CTGCT ATTCACATTGGCTGGTATG-3′, Spry2 forward 5′-CACGG AGTTCAGATGTGTTCTAAGC-3′, Spry2 reverse 5′-ATGT TTGTGCTGAGTGGAGGGG-3′, Spry3 forward 5′-AGCA ATGATTATGTGGAACGGC-3′, Spry3 reverse 5′-TTCTCC CTTCAGAGCACCATCG-3′, Spry4 forward 5′-TCGGGT TCGGGGATTTACAC-3′, Spry4 reverse 5′-GGCTGGTC TTCATCTGGTCAATG-3′.The primers for GAP-43 were designed by Applied Biosystems (TaqMan Gene Signature Mm00500404_m1).

Surgical Procedures and Behavioral Experiments

All *in vivo* experiments were performed with the approval of the ethical commission of the Austrian government (BMWF-66.011/0086-II/10b/2010). The guidelines of the EU concerning animal care were closely observed. Spry2$^{+/-}$ mice weighing approximately 30 g were used (8–12 weeks of age). The cages were housed in a temperature and humidity controlled room with 12/12 h light/dark cycles and animals fed with standard chow and water ad libitum.

Mice were anesthetized (6–8 mg/kg body weight of Xylazin and 90–120 mg/kg body weight of Ketamine) followed by exposure of the sciatic nerve at upper thigh level. The nerve was crushed with a defined force of 1.9 *N* for 2 × 1 min using a feedback controlled electronic squeezer (rodent pincher, Bioseb) at two adjacent sites. Following wound closure and recovery from surgery, the mice were behaviorally analyzed by several testing protocols twice per week (always by the same person). The paw withdrawal latency in response to an increasing heat stimulus at the plantar side of the hindpaw was measured (Hargreaves' test). Mechanical sensitivity (von Frey's test) was tested after application of fine-gauge metal wires of different forces. For testing mainly motor function, the time was measured that an animal stays on an accelerating rod (rotarod) as a measure of balance, coordination, and motor-planning. One week before nerve surgery all of the animals were accustomed to the testing apparatus. Animals were coded so that investigators conducting the behavioral and histological assessments were blind to the treatment conditions.

Nerve Histology

Mice were euthanatized at day 28 postoperatively, and 5 mm of the sciatic nerve distal to the lesioned side removed. The samples were fixed in 4% PFA and 2.5% glutaraldehyde, embedded in Glauerts' resin and prepared for quantitative analysis of myelinated nerve fibers (Raimondo et al., 2009). Series of semithin transverse sections (2.5 μm) were cut using an Ultracut microtome (Leica Microsystems) and stained with toluidine blue. In each nerve, design-based quantitative morphology was performed.

On one randomly selected toluidine-blue-stained semithin section, the total cross-sectional area of the whole nerve was measured using light microscopy. Applying a semiautomatic morphometry program, (MetaMorph, Visitron) the total fiber number, the circle-fitting diameter of the fiber, and the axon as well as myelin thickness were determined. For analysis of unmeylinated fibers, transmission electron microscopy was performed. The number of unmyelinated fibers, myelinating Schwann cells, and unmyelinating Schwann cells was quantified in defined areas (12.2 × 16.2 μm^2) at 8000 fold magnification selected by a systematic random sampling protocol. In each sampling field, the edge effect was avoided using a two-dimensional dissector procedure based on sampling the tops of fibers or nuclei. The mean fiber density was calculated by dividing the total number of fibers within the sampling field by its area. The total number of fibers was estimated by multiplying the mean fiber density with the total cross-sectional area of the whole nerve section.

Statistical Analysis

Statistical analysis was performed using one-way ANOVA followed by Tukey's *post hoc* test or Mann-Whitney test if appropriate. All data points are presented as mean values ± SD or SEM applying Prism or Sigma Stat software. For testing rotarod data over time, a linear regression was fitted. An exponential function was applied for describing the learning curve of nonlesioned mice. Data from behavioral tests were subjected to two-way repeated measures analysis of variance with multicomparison *post hoc* tests. Differences between groups were considered statistically significant if $p < 0.05$ ($^*p < 0.05$, $^{**}p < 0.01$, or $^{***}p < 0.001$).

RESULTS

Peripheral Innervation in Spry2 Knockout Mice

Homozygous Spry2 knockout mice 6–8 weeks of age were smaller (appr. 50% reduction in body weight) than their wildtype (wt) or heterozygous littermates

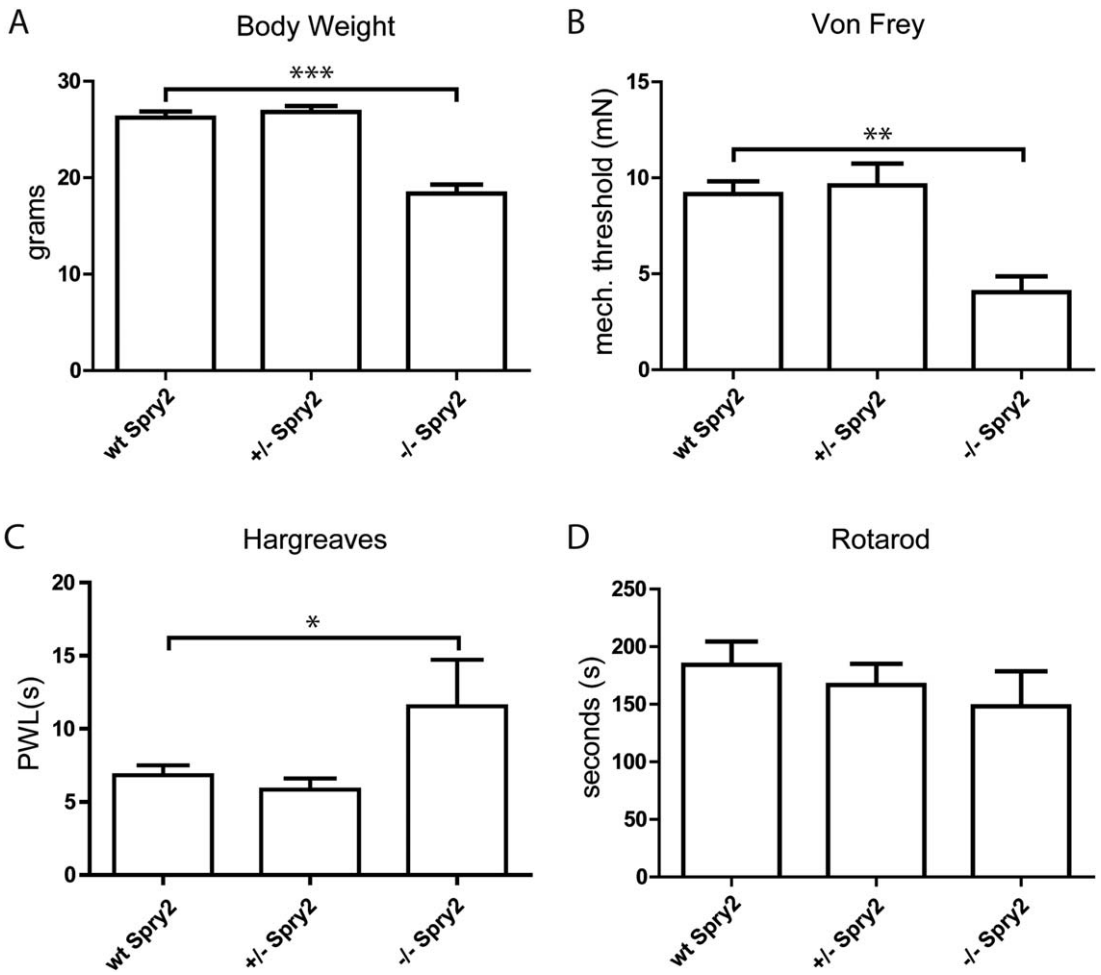

Figure 1 Comparison of body weight of young adult Spry2 deficient mice and behavioral testing. Spry2$^{-/-}$ mice are significantly smaller in comparison with wt or Spry2$^{+/-}$ mice (A; mean ± SEM of $n > 6$ mice per group). Sensory tests reveal a lowered mechanical threshold in response to von Frey hairs (B), but an increased thermal threshold as indicated by the paw withdrawal latency (PWL) following a heat stimulus in homozygous Spry2 knockout mice (C). A statistically nonsignificant trend toward reduced motor coordination was observed on the rotarod treadmill (accelerating mode) in Spry2 deficient mice (D). Mean ± SEM of $n > 6$ mice per group.

[Fig. 1(A)]. The homozygous mice did not even survive mild anesthesia required for surgery. Therefore, they were used for cell culture, behavioral testing, and tissue extraction, but not for nerve lesion experiments.

The threshold for responding to von Frey filaments was reduced indicating higher mechanosensitivity in homozygous Spry2 mice [Fig. 1(B)], whereas thermonociception was impaired [Fig. 1(C)]. The rotarod treadmill test for motor coordination and balance did not reveal statistically significant differences between the three groups [Fig. 1(D)].

The behavioral differences in sensory tests were accompanied by changes in skin innervation and in axon numbers in the sciatic nerve. Comparison of the distribution of nociceptive C-fiber terminals in the glabrous skin of WT and Spry2$^{-/-}$ mice using the pan-neuronal marker PGP9.5 revealed an increase in the total length of nerve endings [NE; Fig. 2(A,B)]. This was due to a thickening of the epidermis which may have been caused by enhanced proliferation of keratinocytes in this global Spry2 knockout mouse model (Mason et al., 2006). Quantitative measurements of the total number of nerve endings in the epidermis (per section area) revealed no difference between genotypes (2.75 ± 0.12 NE/1000 μm^2 for wt and 2.91 ± 0.04 NE/1000 μm^2 for Spry2$^{-/-}$ mice), that is, the density was unchanged. However, a 1.5-fold increase of free nerve ending length was observed in Spry2$^{-/-}$ animals [Fig. 2(B); 88.3 ± 3.5

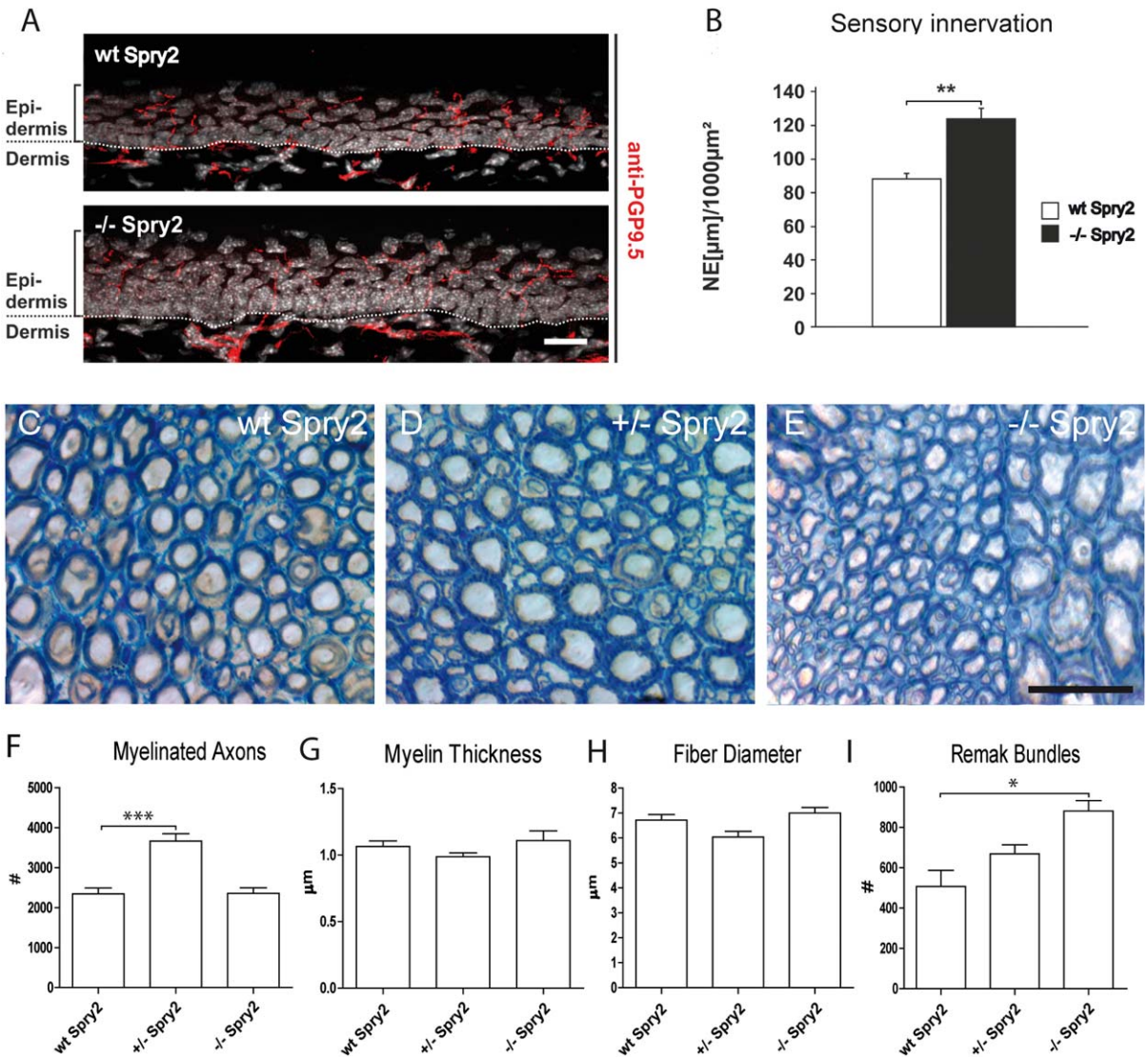

Figure 2 Labeling of axons in the epidermis using a pan-neuronal marker (PGP9.5) and Hoechst stain to identify nuclei demonstrate an increased total length of nerve endings (per area) in the skin of Spry2$^{-/-}$ mice which is due to an enhanced epidermal thickness (A,B). Histomorphological analysis of the sciatic nerve demonstrates myelinated axons in LM images (C–E). More myelinated axons are found in Spry2$^{+/-}$ nerves (F), but myelin thickness (G) and fiber diameters (H) are not affected in either Spry2 genotype as compared to wt. Note the uneven distribution of small- and large-sized myelinated axons in sciatic nerves of Spry2$^{-/-}$ nerves (E). While the number of myelinated axons is unchanged (F), Remak bundles as a correlate for the number of nonmyelinated axons are more frequently observed in Spry2$^{-/-}$ mice (I). Mean ± SEM of $n > 4$ mice per group. Bar = 40 μm (B) or 20 μm (C–E)

μm/1000 μm^2 for wt and 124 ± 6.6 μm/1000 μm^2 for Spry2$^{-/-}$ mice; $^{**}p < 0.01$].

Morphometric analysis of the sciatic nerve [Fig. 2(C–I)] did not reveal differences in number of myelinated axons, in myelin thickness or in fiber diameter of homozygous Spry2 knockout mice, but uneven fiber calibre distributions were detected [Fig. 2(E)]. However, the number of nonmyelinated axons was significantly increased in Spry2$^{-/-}$ mice following quantification of Remak bundles in EM images [containing small-diameter axons surrounded by cytoplasmic processes of a nonmyelinating Schwann cell; Fig. 2(I)]. Conversely, heterozygous Spry2 knockout mice exhibited significantly more

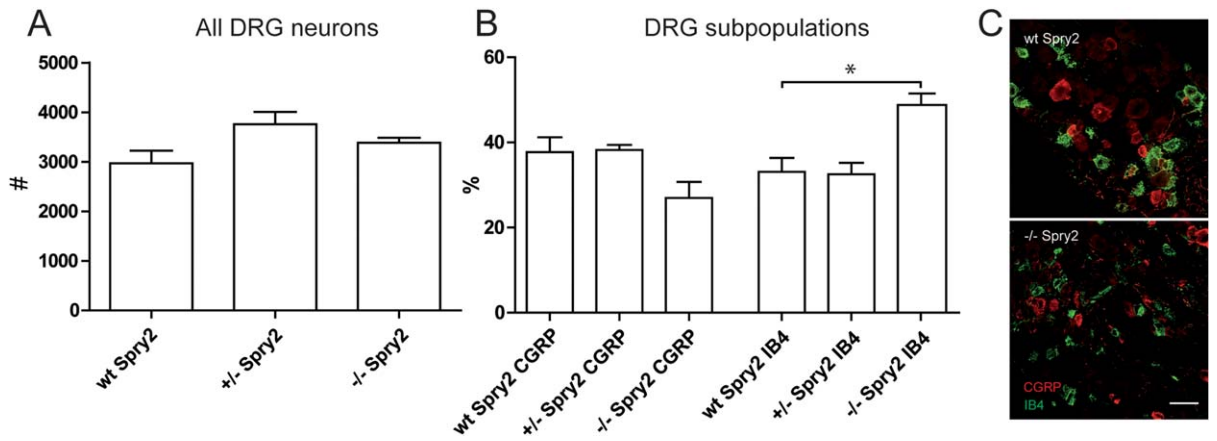

Figure 3 Overall DRG neuron number is not changed in Spry2 deficient mice (A; mean ± SEM of $n > 4$ mice per group). However, CGRP immunoreactive and IB4 binding neurons are differentially distributed in Spry2$^{-/-}$ DRG (B). The relative proportion of CGRP expressing neurons is smaller, while IB4 binding neurons are more frequently observed. Note the reduced size of Spry2 deficient neurons expressing CGRP or binding IB4 in double-labeled confocal images (C). Mean ± SEM of $n > 500$ neurons with $n > 3$ mice per group. Bar = 50 μm.

myelinated axons in sciatic nerves while the number of nonmyelinated axons was only slightly increased [Fig. 2(F,I)].

With regard to muscle innervation the number of motor endplates was nonsignificantly increased in homozygous Spry2 mice (0.2 ± 16% more endplates in Spry2$^{+/-}$ and 10.8 ± 4.4% more endplates in Spry2$^{-/-}$ mice as compared to wt). However, the endplate size was significantly smaller (296 ± 9.9 μm^2 in Spry2$^{-/-}$, 443 ± 13 μm^2 in Spry2$^{+/-}$ and 692 ± 19 μm^2 in wt mice, mean ± SEM of $n = 3$ mice).

Schwann cells and satellite cells in the DRG were devoid of Spry2 immunoreactivity in wt or knockout nerves consistent with our previous observations in the rat DRG (Hausott et al., 2009).

To detect a possible influence of Spry2 reduction on neuron number during development, we analyzed the lumbar DRG (L3, L4, L5) that project into the mouse sciatic nerve. No difference between the genotypes was detected in overall neuron number of the L3–L5 DRG [Fig. 3(A)]. In addition, the total number of lumbar motoneurons in the spinal cord was similar in Spry2 deficient mice as compared to wt (data not shown). Immunohistochemical staining revealed no difference in Spry2 protein levels in small (<500 μm^2) versus large-sized DRG neurons (>500 μm^2). The average Spry2 immunofluorescence intensities (measured in arbitrary units after background correction with background defined as fluorescence detected in Spry2$^{-/-}$ neurons) were 471 ± 28 in small sized and 490 ± 41 in large-sized neurons (mean ± SEM, $n > 30$ per group).

However, the expression of markers for DRG subpopulations changed in Spry2$^{-/-}$ mice with regard to the peptidergic (calcitonin gene-related peptide, CGRP) and nonpeptidergic (IB4) unmyelinated nociceptive neurons, respectively [Fig. 3(B,C)]. While the relative frequency of CGRP positive neurons (mainly thermonociceptive) decreased, the proportion of IB4 binding neurons (mainly mechanosensitive) increased, which may underlie the differences observed in the sensory tests [Fig. 1(B,C)].

Quantitative RT-PCR and Western blot analysis confirmed that Spry2 mRNA and protein levels decrease by 50–60% in DRG of heterozygous Spry2 mice, while no upregulation or downregulation of the other Spry isoforms (Spry1, Spry3, or Spry4) was observed (Supporting Information Fig. 1).

Axon Outgrowth of Spry2 Deficient Neurons in vitro

The increase in epidermal innervation and in nonmyelinated axon numbers in Spry2$^{-/-}$ mice with no elevation in total DRG neuron number suggested that sensory axon branching is enhanced in Spry2 deficient neurons. Therefore, we investigated axon outgrowth of DRG neurons obtained from young adult homozygous and heterozygous Spry2 knockout mice. Dissociated neurons were plated on a growth promoting substrate (poly-L-lysine/laminin) and labeled with anti-tubulin antibodies after 24 h in culture.

Obvious differences were apparent with regard to the axon outgrowth patterns of sensory neurons

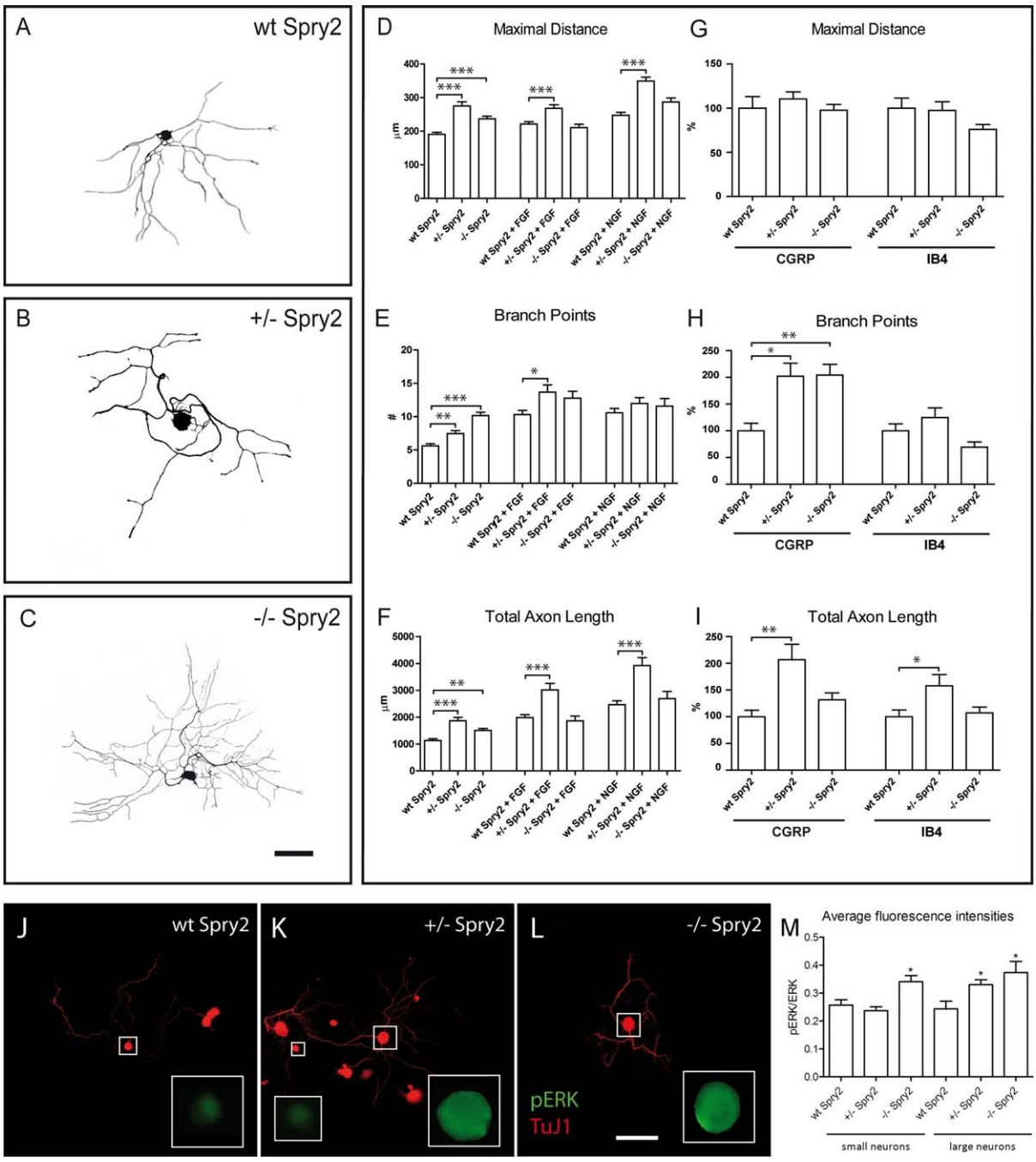

Figure 4 Representative examples of neuronal morphologies of young adult DRG neurons stained for the tubulin marker Tuj-1. Inverted fluorescence images are shown to document the different complexities of the axonal tree (A–C). In cultures obtained from Spry2$^{+/-}$ mice, the length of the longest axon (maximal distance) is significantly increased (D). In contrast, axonal branching is particularly enhanced in untreated Spry2$^{-/-}$ neurons (E). Following treatment with NGF (100 ng/mL), FGF-2 (100 ng/mL), or vehicle for 24 h the total axonal length (F) and axon elongation are promoted mainly in heterozygous Spry2 knockout cultures. Labeling for nonmyelinating neurons reveals that axonal elongation and branching is significantly enhanced in the CGRP positive neuronal subpopulation, whereas IB4 binding neurons are less responsive in Spry2 deficient cultures (G–I). Compared to wt (J) activated ERK levels are significantly increased in DRG neurons dissociated from Spry2$^{+/-}$ (K) or Spry2$^{-/-}$ (L) mice that reveal the highest ratios (pERK/ERK) of fluorescence intensities following background correction (M). Mean ± SEM of $n \geq 3$ independent experiments with a total number of neurons > 80 (D–F), > 40 (G–I) and, > 20 (M) per group. Bar = 100 μm

[Fig. 4(A–C)]. The length of the longest axon per neuron as a measure for the neuronal capacity to induce axon elongation, the total axon length, and the number of axonal branch points were significantly enhanced in both genotypes when compared to wt. However, heterozygous and homozygous Spry2 knockout neurons differed with regard to their axon outgrowth pattern: $Spry2^{+/-}$ neurons exhibited a tendency toward axon elongation [Fig. 4(B,D)], while homozygous neurons revealed an axon branching phenotype [Fig. 4(C,E)]. The effect on total axon length was particularly prominent in $Spry2^{+/-}$ neurons [Fig. 4(F)]. Axon outgrowth and elongation were further enhanced by basic FGF-2 and, particularly, following treatment with NGF [Fig. 4(D,F)]. Both factors induce axon branching already in wt cultures [Klimaschewski et al., 2004, Fig. 4(E)]. Homozygous Spry2 knockout neurons did not exhibit significantly increased axon outgrowth in response to growth factor treatment.

The prominent elongative axon outgrowth effect in $Spry2^{+/-}$ neurons was also visible in another type of primary neuron culture. As demonstrated in Supporting Information Fig. 2, dissociated sympathetic SCG $Spry2^{+/-}$ neurons extended significantly longer axons with no change in number of axonal branch points.

Neuronal subpopulations in DRGs responded differently to reduced levels of Spry2. We observed that large diameter neurons exhibited stronger effects than small-diameter neurons with regard to axon elongation by $Spry2^{+/-}$ neurons and branching by $Spry2^{-/-}$ neurons as compared to wt (data not shown). Furthermore, Spry2 deficient CGRP positive neurons displayed enhanced total axon outgrowth with significantly elevated maximal distance and numbers of axon branch points. Conversely, the axon growth promoting effects in IB4 binding Spry2 knockout neurons were weaker [Fig. 4(G–I)], probably because IB4-binding neurons are limited in their regenerative capacity *in vitro* (Leclere et al., 2007). Nerve lesion *in vivo* promotes axon growth primarily in myelinated DRG neurons, but not in IB4-binding small nonmyelinated neurons (Belyantseva and Lewin, 1999).

A possible correlation of the enhanced axon outgrowth in Spry2 deficient neurons with changes in ERK activation was investigated by immunofluorescence applying pERK and ERK antibodies. As outlined in the Introduction, downregulation of Spry2 leads to the activation of Ras and ERK, whereas phosphorylation of AKT and p38 remains unaffected (Hausott et al., 2009). In comparison to wt, Spry2 deficient neurons exhibited increased basal pERK activity in neuronal cell bodies 2 h and 24 h after plating [Fig. 4(J–L)]. Intensity measurements revealed elevated pERK/ERK ratios in large $Spry2^{+/-}$ neurons and in large as well as small $Spry2^{-/-}$ neurons [Fig. 4(M)]. Treatment with NGF or FGF-2 stimulated ERK phosphorylation in both genotypes with no changes in pAKT/AKT levels (data not shown).

Peripheral Axon Regeneration in Heterozygous Spry2 Knockout Mice

From the *in vitro* data, we hypothesized that moderately reduced Spry2 levels may promote axon regeneration of sensory and motor neurons that express Spry2 as well (Chambers and Mason, 2000). Therefore, the sciatic nerve crush model was applied to study peripheral nerve regeneration in $Spry2^{+/-}$ mice *in vivo*. As stated above, homozygous Spry2 mice could not be used as they did not recover from anesthesia required for nerve surgery.

Histological analysis of the sciatic nerve was performed 28 days after injury distal to the crush site [Fig. 5(A,B)]. Stereological methods were applied to count myelinated fibers and to measure myelin thickness. Following crush injury, the overall diameter of the distal sciatic nerve [Fig. 5(C)] and the number of myelinated axons [Fig. 5(D)] increased significantly, while myelin thickness was not affected [Fig. 5(E)]. Axon diameters decreased in lesioned $Spry2^{+/-}$ knockout animals but this was statistically not significant [Fig. 5(B,F)]. The number of Remak bundles (Schwann cells enwrapping nonmyelinated axons) was elevated with no change in the number of axons per Remak bundle (507 ± 80 in wt vs. 669 ± 45 in $Spry2^{+/-}$ mice, mean $\pm$ SEM of $n = 3$ mice).

Before nerve injury and during nerve regeneration the mice were tested behaviorally at regular intervals. The baseline values in rotarod (sensomotor), von Frey's (mechanosensation), or Hangreaves' tests (nociception) were not changed in $Spry2^{+/-}$ mice as compared to wt littermates [Figs. 1 and 6(A–D)]. However, significant differences between heterozygous knockout and wt mice were observed 3 weeks after lesion on the accelerating rotarod which corresponds to the time period myelinated axons require to reinnervate distal leg muscles. Following sciatic nerve lesion, $Spry2^{+/-}$ mice improved their performance by 2.9 ± 0.5 % per day, whereas wt mice improved only by 1.9 ± 0.4% per day [Fig. 6(A)]. To rule out different motor learning capabilities between the two groups, nonlesioned mice of both genotypes were subjected to 10 days of consecutive rotarod tests. No significant differences in performance were apparent [Fig. 6(B)]. Recovery of somatosensory function was not affected following injury supporting our observation that mainly myelinated axons regenerated faster in $Spry2^{+/-}$ mice [Fig. 6(C,D)]. Furthermore, regeneration of motor neurons was analyzed by endplate labeling in

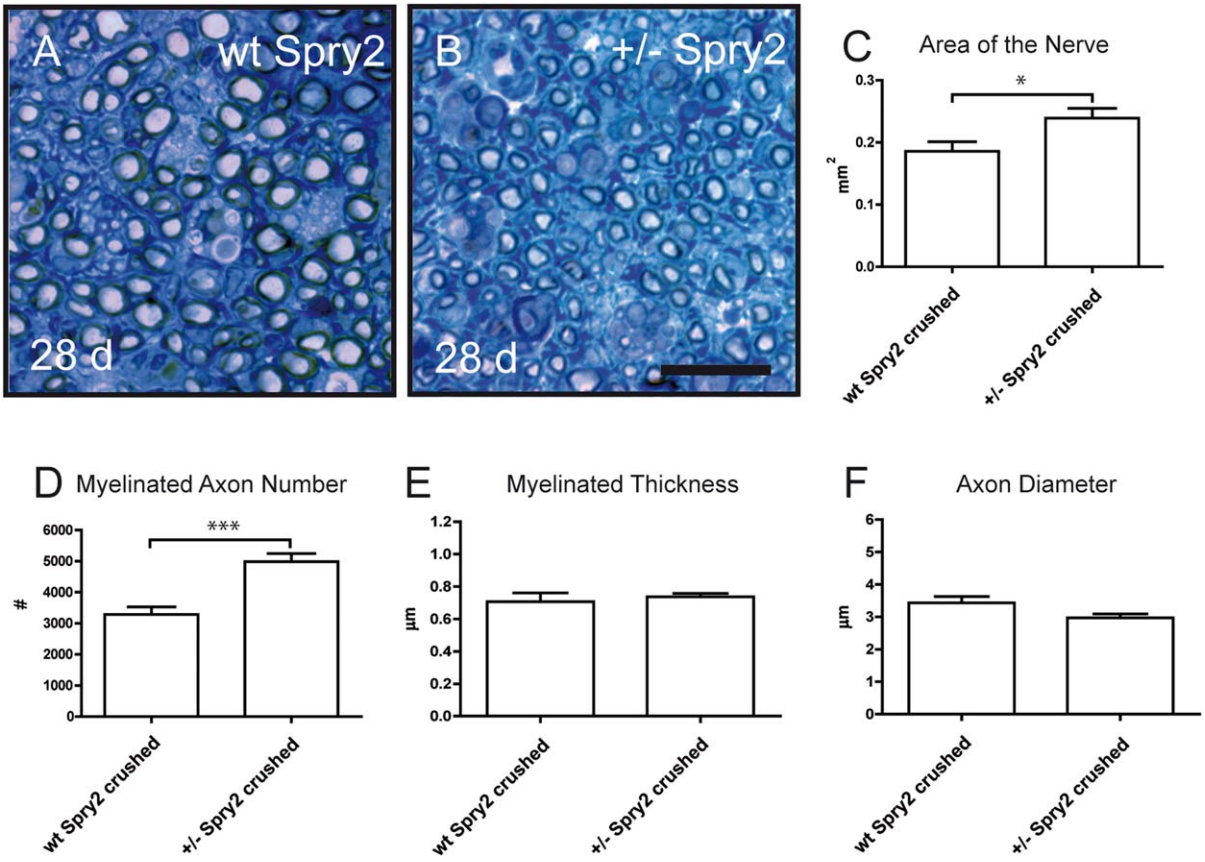

Figure 5 Histomorphological analysis of toluidine blue stained myelinated axons in the sciatic nerve (A,B) 4 weeks after nerve crush in Spry2$^{+/-}$ mice (A,B). The diameter of regenerated nerves is larger (C) which is due to an increase in number of myelinated axons (D) with no change in myelin thickness (E). A nonsignificant trend toward smaller axon diameters is observed in heterozygous knockout nerves (B,F). Mean ± SEM of $n > 6$ mice per group. Bar = 20 μm

distal leg muscles. Alpha-bungarotoxine (BTX) staining of the gastrocnemius muscle 4 weeks after surgery revealed a higher density of motor endplates in Spry2$^{+/-}$ mice as compared to wt [Fig. 6(E–G)]. The results suggest that Spry2$^{+/-}$ mice exhibit improved recovery due to faster axon regeneration of mainly myelinated axons as no differences were observed in nociceptive/mechanosensory testing paradigms involving mainly nonmyelinated axons.

Improved Long-Distance Regeneration is Accompanied by Increased Axonal GAP-43 in Spry2$^{+/-}$ Mice

Regarding possible mechanisms of Spry2 inhibition, we investigated mRNAs for GAP-43 and β-actin in the sciatic nerve by qRT-PCR. Local translation of these axonal mRNAs regulates specific modes of axon regeneration. Axonally targeted GAP-43 mRNA increases axon length, whereas axonally targeted β-actin stimulates axon branching of sensory neurons (Donnelly et al., 2013). In fact, GAP-43 mRNA was significantly upregulated 2 weeks after lesion in the distal sciatic nerve of Spry2$^{+/-}$ mice as compared to wt [Fig. 7(A)]. This was accompanied by a statistically nonsignificant trend toward increased axonal GAP-43 immunostaining in Spry2$^{+/-}$ mice distal to the crush site [Fig. 7(B,C)]. It has to be taken into account, however, that axonally transported GAP-43 mRNA is translated mainly in the tip of the axon, and the protein is transported anterogradely and present at higher levels in the growth cone than in the axon shaft (Meiri et al., 1988, Tetzlaff et al., 1989). No differences were observed with regard to β-actin mRNA between Spry2$^{+/-}$ and wt nerves.

DISCUSSION

In this study, evidence is provided that reduction of Spry2, a negative feedback inhibitor of receptor

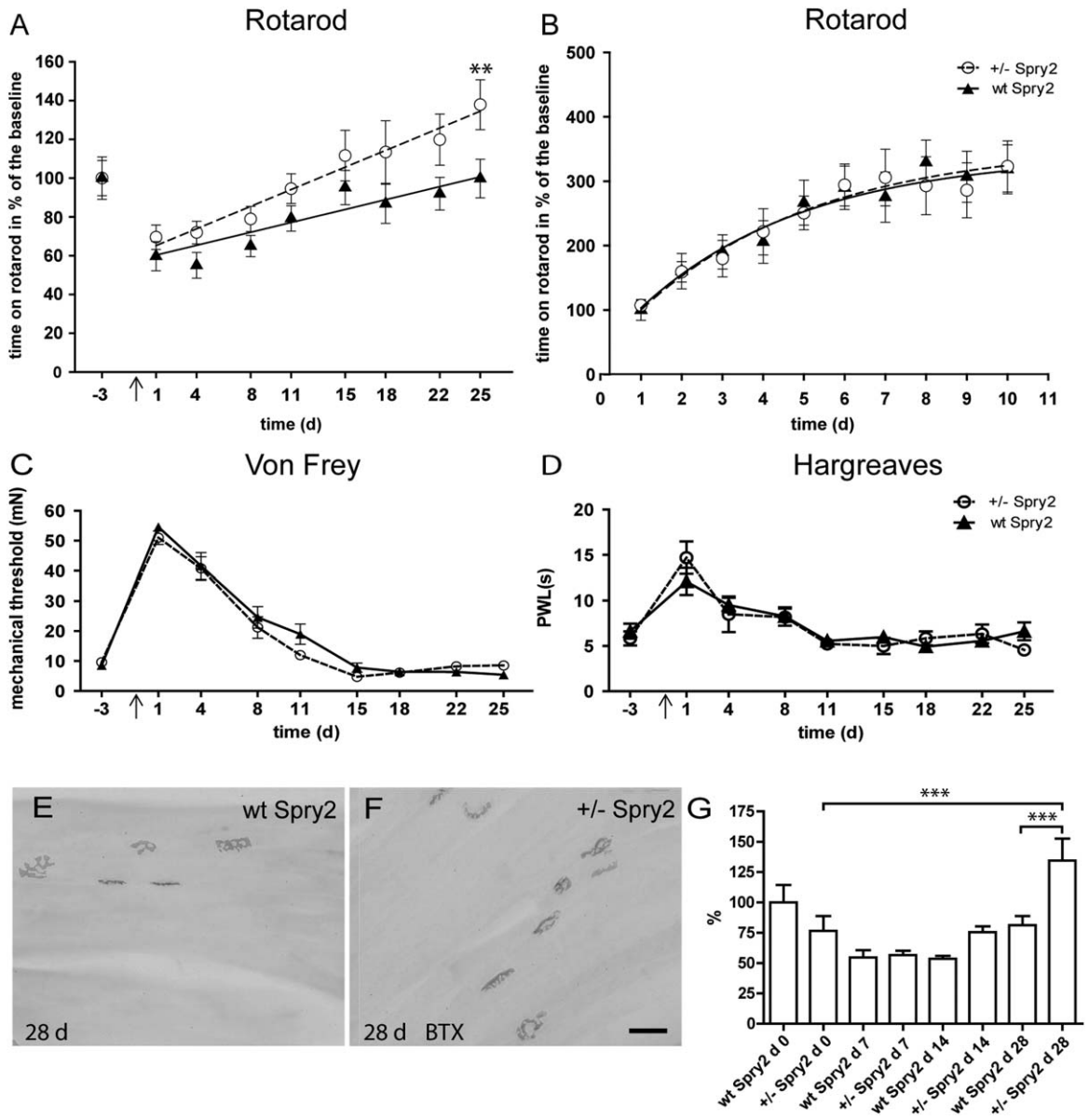

Figure 6 Functional recovery following sciatic nerve crush lesion in Spry2$^{+/-}$ mice and wt littermates. Treadmill running (rotarod) reveals that Spry2$^{+/-}$ mice regenerate significantly faster than wt mice (A). Motor learning was comparable during a 10-day training period in nonlesioned animals (B). Sensory tests analyzing the mechanical threshold in response to von Frey hairs (C) or the pain threshold as paw withdrawal latency following a thermal stimulus (D) did not exhibit significant differences (mean ± SEM of $n > 10$ mice per group, arrow indicates time of injury). Alpha-bungarotoxine (BTX) staining (E,F) in the gastrocnemius muscle demonstrates a significantly higher density of motor endplates in Spry2$^{+/-}$ mice 4 weeks after injury (G). Mean ± SEM of $n > 3$ independent experiments. Bar = 45 μm

tyrosine kinase signaling, stimulates axon outgrowth *in vitro* and *in vivo*. For the first time, we demonstrate that the two main modes of axon growth, elongation and branching, depend on neuronal Spry2 levels *in vivo*.

Following sciatic nerve crush lesion, motor performance improves faster in Spry2$^{+/-}$ mice than in wt controls. This observation may be attributed to higher numbers of regenerating myelinated axons as well as muscle endplates and, at the molecular level, to an induction of GAP-43, a downstream target of ERK signaling (Murakami et al., 2011). Reduction of Spry2 levels appears to affect predominantly large-

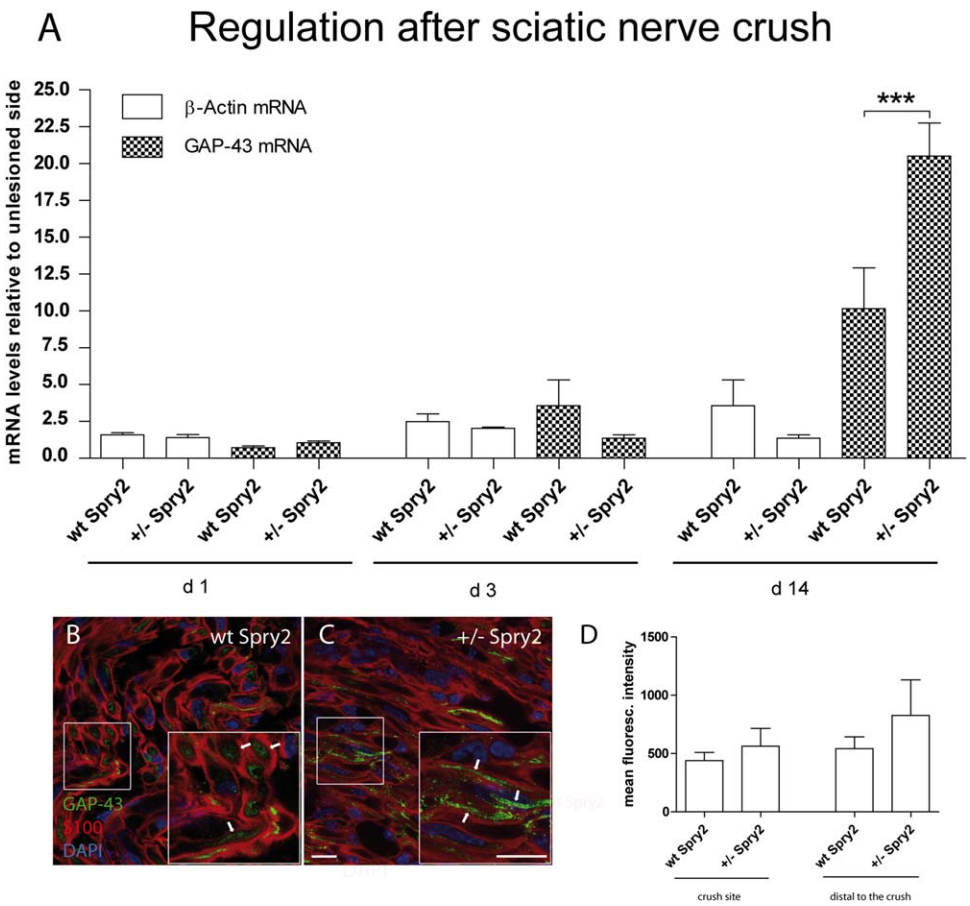

Figure 7 Expression analysis of GAP-43 and β-actin mRNA in the distal sciatic nerve at 1, 3, and 14 days following a nerve crush lesion (A). Values are compared to the contralateral side and normalized to nonlesioned nerves. Mean ± SEM of $n = 3$ nerves per group. Transient upregulation of β-actin mRNA is accompanied by prominent upregulation of GAP-43 mRNA 2 weeks after lesion in Spry2$^{+/-}$ mice. Sciatic nerve sections obtained 2 weeks after crush injury reveal axonal (S100 negative) GAP-43 immunostaining (arrows in B and C). Fluorescence measurements indicate a statistically nonsignificant trend toward increased GAP-43 levels in axons at 5 mm distal to the crush site (mean ± SEM of $n = 3$ mice). Bars = 25 μm

sized motor and sensory (presumably proprioceptive) neurons required for successful restoration of muscle activity. Taken together, these findings are in accordance with our previous work demonstrating that siRNA mediated downregulation of Spry2 significantly enhances axon elongation of peripheral and central neurons *in vitro* (Hausott et al., 2009; Hausott et al., 2012). They indicate that moderate reductions of Spry2 positively affect axonal regeneration in the peripheral and possibly also in the central nervous system.

Spry2 inhibits the Ras/Raf/MEK/ERK cascade downstream of growth factor activated receptor tyrosine kinases. This pathway is a key regulator of axon outgrowth during development (Markus et al., 2002a), although some aspects of early DRG and motor neuron development were found to be ERK1/2 independent (Newbern et al., 2011). Activated receptors signal via adaptor proteins, the GDP-GTP exchange factor SOS and the small GTPase Ras. Ras, in turn, stimulates the serine/threonine kinase Raf1 (MAPK kinase kinase), MEK1/2 (MAPK kinase), and ERK1/2 (MAPK). Activated ERK1/2 is involved in the translation of various axonal mRNAs and influences gene expression via phosphorylation of transcription factors (Zhou and Snider, 2006). Target genes of ERK include GAP-43 and Sprys themselves which translocate to the plasma membrane and are phosphorylated by Src kinase (Mason et al., 2006).

ERK is required for axotomy-induced growth cone formation after lesion (Chierzi et al., 2005) and for axon growth of preaxotomized DRG explants, which

model *in vivo* conditions controlled by growth factors (Wiklund et al., 2002). Local axon assembly depends on ERK activity via modifications of axonal microtubules, actin filaments and changes in local protein translation in a growth factor dependent manner (Atwal et al., 2000; Campbell and Holt, 2003; Goold and Gordon-Weeks, 2005). Blockade of ERK results in depolymerization of actin and in the collapse of growth cones (Atwal et al., 2003). However, ERK inhibitors apparently exert no effect on spontaneous axon outgrowth of adult DRG explants, while neurotrophic factor induced growth is significantly impaired (Sondell et al., 1999; Sjogreen et al., 2000).

In addition to ERK, the activation of phosphatidylinositol 3-kinase (PI3K) plays a key role in axonal elongation, branching, and gene expression underlying axon maintenance (Zhou and Snider, 2006). PI3K/AKT activity is not influenced by Spry2 downregulation in adult peripheral neurons (Hausott et al., 2009), but increases axon caliber and branching following stimulation with growth factors in embryonic DRG neurons (Markus et al., 2002b). Growth factors like FGF-2 promote axon elongation by inducing stronger activation of ERK than of AKT, whereas NGF treatment primarily promotes axon branching and results in both, ERK- and AKT-phosphorylation, to a similar extent (Klimaschewski et al., 2004).

Spry2 deficient mice are expected to reflect the phenotype of overexpressing neurotrophic factors with regard to ERK signaling. For example, FGF-2 overexpressing mice (Jungnickel et al., 2006) and $Spry2^{+/-}$ mice both reveal increased numbers of regenerating myelinated axons after sciatic nerve crush. However, no improvement in functional recovery was observed in FGF-2 transgenic mice suggesting differences in axon branching and/or myelination between the two mouse models. While Spry2 deficient mice did not exhibit significant changes in myelination, FGF-2 overexpression resulted in reduced myelin thickness most likely because of FGF-2 mediated dedifferentiation and proliferation of Schwann cells which lack Spry2.

The axon branching phenotype observed particularly in homozygous Spry2 knockout cultures may be involved in developmental changes of peripheral sensory innervation. The increased number of free nerve endings in the epidermis (indicating enlarged receptive fields) combined with a higher number of non-myelinated axons in the sciatic nerve and a greater proportion of IB4 binding neurons in the DRG suggest a lowered mechanosensitive threshold as observed in von Frey testing. IB4 positive neurons express receptors for glial-cell-line-derived neurotrophic factor and have been shown to be particularly sensitive to Spry2 deficiency (Taketomi et al., 2005). Moreover, they play a major role in mechanosensation (Molliver et al., 1997) and project to the epidermis (Zylka et al., 2005). In contrast, the thermonociceptive threshold was elevated in $Spry2^{-/-}$ mice probably due to a diminished innervation of the skin by CGRP positive fibers (which our antibody was unable to detect). The CGRP-positive neuron population corresponds almost exactly with the NGF responsive, TrkA-expressing neuron population and is mainly involved in thermonociception (Averill et al., 1995). In support of this hypothesis, we observed a trend toward reduced numbers of CGRP positive small DRG neurons suggesting that in homozygous Spry2 knockout mice nociception may be perturbed.

In conclusion, this study reveals that Spry2 plays an important role in limiting axon outgrowth during development and nerve regeneration. ERK signaling and downstream GAP-43 mRNA levels are enhanced in $Spry2^{+/-}$ neurons. The induction of GAP-43 following nerve injury plays a key role in stimulation of axon elongation without affecting axon branching (Donnelly et al., 2013). Therefore, downregulation or pharmacological inhibition of Spry2 may emerge as a novel approach to promote long-distance regeneration and faster reinnervation following injury in the peripheral nervous system.

We are grateful to Rudolf Glueckert for help with the mouse breeding, to Katrin Braun for help with neuron culture experiments, and to Andreas Frei and Aglaja Waibl for help with image analysis.

REFERENCE

Abercrombie M. 1943. Estimation of nuclear population from microtome sections. Anat Rec 94:239–247.

Andratsch M, Mair N, Constantin CE, Scherbakov N, Benetti C, Quarta S, Vogl C, et al. 2009. A key role for gp130 expressed on peripheral sensory nerves in pathological pain. J Neurosci 29:13473–13483.

Atwal JK, Massie B, Miller FD, Kaplan DR. 2000. The TrkB-Shc site signals neuronal survival and local axon growth via MEK and PI3-kinase. Neuron 27:265–277.

Atwal JK, Singh KK, Tessier-Lavigne M, Miller FD, Kaplan DR. 2003. Semaphorin 3F antagonizes neurotrophin-induced phosphatidylinositol 3-kinase and mitogen-activated protein kinase kinase signaling: A mechanism for growth cone collapse. J Neurosci 23: 7602–7609.

Averill S, McMahon SB, Clary DO, Reichardt LF, Priestley JV. 1995. Immunocytochemical localization of trkA receptors in chemically identified subgroups of adult rat sensory neurons. Eur J Neurosci 7:1484–1494.

Baumer BE, Kurz A, Borrie SC, Sickinger S, Dours-Zimmermann MT, Zimmermann DR, Bandtlow CE.

2014. Nogo receptor homolog NgR2 expressed in sensory DRG neurons controls epidermal innervation by interaction with Versican. J Neurosci 34:1633–1646.

Bavassano C, Marvaldi L, Langeslag M, Sarg B, Lindner H, Klimaschewski L, Kress M, et al. 2013. Identification of voltage-gated K^+ channel beta 2 (Kvbeta2) subunit as a novel interaction partner of the pain transducer Transient Receptor Potential Vanilloid 1 channel (TRPV1). Biochim Biophys Acta 1833:3166–3175.

Belyantseva IA, Lewin GR. 1999. Stability and plasticity of primary afferent projections following nerve regeneration and central degeneration. Eur J Neurosci 11:457–468.

Campbell DS, Holt CE. 2003. Apoptotic pathway and MAPKs differentially regulate chemotropic responses of retinal growth cones. Neuron 37:939–952.

Chambers D, Mason I. 2000. Expression of sprouty2 during early development of the chick embryo is coincident with known sites of FGF signalling. Mech Dev 91:361–364.

Chierzi S, Ratto GM, Verma P, Fawcett JW. 2005. The ability of axons to regenerate their growth cones depends on axonal type and age, and is regulated by calcium, cAMP and ERK. Eur J Neurosci 21:2051–2062.

Donnelly CJ, Park M, Spillane M, Yoo S, Pacheco A, Gomes C, Vuppalanchi D, et al. 2013. Axonally synthesized beta-actin and GAP-43 proteins support distinct modes of axonal growth. J Neurosci 33:3311–3322.

Gallo G. 2011. The cytoskeletal and signaling mechanisms of axon collateral branching. Dev Neurobiol 71:201–220.

Goold RG, Gordon-Weeks PR. 2005. The MAP kinase pathway is upstream of the activation of GSK3 beta that enables it to phosphorylate MAP1B and contributes to the stimulation of axon growth. Mol Cell Neurosci 28: 524–534.

Gordon T. 2009. The role of neurotrophic factors in nerve regeneration. Neurosurg Focus 26:E3.

Gross I, Bassit B, Benezra M, Licht JD. 2001. Mammalian sprouty proteins inhibit cell growth and differentiation by preventing ras activation. J Biol Chem 276:46460–46468.

Hanafusa H, Torii S, Yasunaga T, Nishida E. 2002. Sprouty1 and Sprouty2 provide a control mechanism for the Ras/MAPK signalling pathway. Nat Cell Biol 4:850–858.

Hausott B, Vallant N, Auer M, Yang L, Dai F, Brand-Saberi B, Klimaschewski L. 2009. Sprouty2 down-regulation promotes axon growth by adult sensory neurons. Mol Cell Neurosci 42:328–340.

Hausott B, Vallant N, Schlick B, Auer M, Nimmervoll B, Obermair GJ, Schwarzer C, et al. 2012. Sprouty2 and −4 regulate axon outgrowth by hippocampal neurons. Hippocampus 22:434–441.

Impagnatiello MA, Weitzer S, Gannon G, Compagni A, Cotten M, Christofori G. 2001. Mammalian sprouty-1 and −2 are membrane-anchored phosphoprotein inhibitors of growth factor signaling in endothelial cells. J Cell Biol 152:1087–1098.

Jungnickel J, Haase K, Konitzer J, Timmer M, Grothe C. 2006. Faster nerve regeneration after sciatic nerve injury in mice over-expressing basic fibroblast growth factor. J Neurobiol 66:940–948.

Klimaschewski L, Hausott B, Angelov DN. 2013. The pros and cons of growth factors and cytokines in peripheral axon regeneration. Int Rev Neurobiol 108:137–171.

Klimaschewski L, Nindl W, Feurle J, Kavakebi P, Kostron H. 2004. Basic fibroblast growth factor isoforms promote axonal elongation and branching of adult sensory neurons in vitro. Neuroscience 126:347–353.

Klimaschewski L, Nindl W, Pimpl M, Waltinger P, Pfaller K. 2002. Biolistic transfection and morphological analysis of cultured sympathetic neurons. J Neurosci Methods 113:63–71.

Leclere PG, Norman E, Groutsi F, Coffin R, Mayer U, Pizzey J, Tonge D. 2007. Impaired axonal regeneration by isolectin B4-binding dorsal root ganglion neurons in vitro. J Neurosci 27:1190–1199.

Loy B, Apostolova G, Dorn R, McGuire VA, Arthur JS, Dechant G. 2011. p38alpha and p38beta mitogen-activated protein kinases determine cholinergic transdifferentiation of sympathetic neurons. J Neurosci 31: 12059–12067.

Markus A, Patel TD, Snider WD. 2002a. Neurotrophic factors and axonal growth. Curr Opin Neurobiol 12:523–531.

Markus A, Zhong J, Snider WD. 2002b. Raf and Akt mediate distinct aspects of sensory axon growth. Neuron 35: 65–76.

Mason I. 2007. Initiation to end point: The multiple roles of fibroblast growth factors in neural development. Nat Rev Neurosci 8:583–596.

Mason JM, Morrison DJ, Basson MA, Licht JD. 2006. Sprouty proteins: Multifaceted negative-feedback regulators of receptor tyrosine kinase signaling. Trends Cell Biol 16:45–54.

Meiri KF, Willard M, Johnson MI. 1988. Distribution and phosphorylation of the growth-associated protein GAP-43 in regenerating sympathetic neurons in culture. J Neurosci 8:2571–2581.

Molliver DC, Wright DE, Leitner ML, Parsadanian AS, Doster K, Wen D, Yan Q, et al. 1997. IB4-binding DRG neurons switch from NGF to GDNF dependence in early postnatal life. Neuron 19:849–861.

Murakami M, Ito H, Hagiwara K, Kobayashi M, Hoshikawa A, Takagi A, Kojima T, et al. 2011. Sphingosine kinase 1/S1P pathway involvement in the GDNF-induced GAP43 transcription. J Cell Biochem 112:3449–3458.

Newbern JM, Li X, Shoemaker SE, Zhou J, Zhong J, Wu Y, Bonder D, et al. 2011. Specific functions for ERK/MAPK signaling during PNS development. Neuron 69: 91–105.

Raimondo S, Fornaro M, Di Scipio F, Ronchi G, Giacobini-Robecchi MG, Geuna S. 2009. Methods and protocols in peripheral nerve regeneration experimental research: Part II - Morphological techniques. In: Stefano Geuna, Pierluigi Tos and Bruno Battiston (eds) Int Rev Neurobiol 81–103.

Rishal I, Golani O, Rajman M, Costa B, Ben-Yaakov K, Schoenmann Z, Yaron A, et al. 2013. WIS-NeuroMath enables versatile high throughput analyses of neuronal processes. Dev Neurobiol 73:247–256.

Sasaki A, Taketomi T, Wakioka T, Kato R, Yoshimura A. 2001. Identification of a dominant negative mutant of Sprouty that potentiates fibroblast growth factor- but not epidermal growth factor-induced ERK activation. J Biol Chem 276:36804–36808.

Sjogreen B, Wiklund P, Ekstrom PA. 2000. Mitogen activated protein kinase inhibition by PD98059 blocks nerve growth factor stimulated axonal outgrowth from adult mouse dorsal root ganglia in vitro. Neuroscience 100: 407–416.

Sondell M, Lundborg G, Kanje M. 1999. Vascular endothelial growth factor has neurotrophic activity and stimulates axonal outgrowth, enhancing cell survival and Schwann cell proliferation in the peripheral nervous system. J Neurosci 19:5731–5740.

Strickland IT, Richards L, Holmes FE, Wynick D, Uney JB, Wong LF. 2011. Axotomy-induced miR-21 promotes axon growth in adult dorsal root ganglion neurons. PLoS One 6:e23423.

Taketomi T, Yoshiga D, Taniguchi K, Kobayashi T, Nonami A, Kato R, Sasaki M, et al. 2005. Loss of mammalian Sprouty2 leads to enteric neuronal hyperplasia and esophageal achalasia. Nat Neurosci 8:855–857.

Tang N, Marshall WF, McMahon M, Metzger RJ, Martin GR. 2011. Control of mitotic spindle angle by the RAS-regulated ERK1/2 pathway determines lung tube shape. Science 333:342–345.

Tetzlaff W, Zwiers H, Lederis K, Cassar L, Bisby MA. 1989. Axonal transport and localization of B-50/GAP-43-like immunoreactivity in regenerating sciatic and facial nerves of the rat. J Neurosci 9:1303–1313.

Wiklund P, Ekstrom PA, Edstrom A. 2002. Mitogen-activated protein kinase inhibition reveals differences in signalling pathways activated by neurotrophin-3 and other growth-stimulating conditions of adult mouse dorsal root ganglia neurons. J Neurosci Res 67:62–68.

Yu T, Yaguchi Y, Echevarria D, Martinez S, Basson MA. 2011. Sprouty genes prevent excessive FGF signalling in multiple cell types throughout development of the cerebellum. Development 138:2957–2968.

Zhou FQ, Snider WD. 2006. Intracellular control of developmental and regenerative axon growth. Philos Trans R Soc Lond B Biol Sci 361:1575–1592.

Zylka MJ, Rice FL, Anderson DJ. 2005. Topographically distinct epidermal nociceptive circuits revealed by axonal tracers targeted to Mrgprd. Neuron 45:17–25.